A New AUV Navigation System Exploiting Unscented Kalman Filter

B. Allotta[1,3], A. Caiti[2,3], R. Costanzi[1,3], F. Fanelli[1,3], D. Fenucci[2,3], E. Meli[1,3], and A. Ridolfi[1,3]

[1]Mechatronics and Dynamic Modelling Laboratory - MDM Lab, Department of Industrial Engineering Florence - DIEF, University of Florence, Via di Santa Marta 3, 50139, Florence, Italy benedetto.allotta@unifi.it, riccardo.costanzi@unifi.it, francesco.fanelli@unifi.it, enrico.meli@unifi.it, a.ridolfi@unifi.it

[2]Bioengineering and Robotics Research Center, Centro Piaggio, University of Pisa, Largo Lucio Lazzarino 1, 56122 Pisa, Italy andrea.caiti@dsea.unipi.it, d.fenucci@gmail.com

[3]Interuniversity Center of Integrated Systems for the Marine Environment (ISME), www.isme.unige.it

Abstract

The development of precise and robust navigation strategies for Autonomous Underwater Vehicles (AUVs) is fundamental to reach the high level of performance required by complex underwater tasks, often including more than one AUV. One of the main factors affecting the accuracy of AUVs navigation systems is the algorithm used to estimate the vehicle motion, usually based on kinematic vehicle models and linear estimators. A precise and reliable navigation system is indeed fundamental to AUVs: the Global Positioning System (GPS) signal is not available underwater, thus making it very hard to know the position of the vehicle in real-time.

In this paper, the authors present an innovative navigation strategy specifically designed for AUVs, based on the Unscented Kalman Filter (UKF). The new algorithm proves to be effective if applied to this class of vehicles and allows to achieve a satisfying accuracy improvement compared to standard navigation algorithms.

The proposed strategy has been experimentally validated using the navigation data acquired in suitable sea tests performed in Biograd Na Moru (Croatia) in the framework of the FP7 European ARROWS project tests performed during the Breaking the Surface 2014 (BtS 2014) workshop. The vehicles involved are the two Typhoon AUVs, developed and built by the Department of Industrial Engineering of the University of Florence within

the THESAURUS Tuscany Region project for exploration and surveillance of underwater archaeological sites. The experiment, described in the paper, was performed to preliminary test the cooperative navigation between these AUVs. The new algorithm has been initially tested offline, and the validation of the proposed strategy provided accurate results in estimating the vehicle dynamic behaviour.

Keywords: AUVs, Underwater Robotics, Navigation, Marine Robotics, Underwater Vehicles.

---

1. Introduction

Nowadays, Autonomous Underwater Vehicles (AUVs) are widely used in many fields of application: they are employed for scientific purposes (e.g. exploration and surveillance of archaeological sites), to complete industrial tasks at high depths (for instance they are exploited in the Oil&Gas industry), to carry out reconnaissance and patrolling missions in the military field, or even to conduct search and rescue duties.
Regardless of the kind of mission the vehicle is required to execute, the availability of a precise and robust navigation system, i.e. suitable hardware and software components used to estimate in real-time the vehicle pose, is of fundamental importance [16], [18], [4], [11]. Indeed, the high accuracy needed by the imposed tasks, which can even involve multiple vehicles [2], [10], [26], [15] makes motion estimation a key factor in underwater autonomous navigation, requiring precise and computationally lightweight estimation algorithms. The quality of the navigation system not only influences the results of the performed mission in terms of position error between the desired and the executed path, but also affects the outcome of the georeferencing process of the data acquired by the onboard sensors; this is especially important in archaeology, history or anthropology-related missions (e.g. the exploration of ancient wrecks).
In addition to the intrinsic difficulties of the localization task, the underwater environment poses additional limitations that further complicate the estimation process: for instance, the Global Positioning System (GPS) signal is not available underwater, making it very hard to estimate the vehicle position. This increases the need for a precise and robust navigation system.
The vast majority of the motion estimation filters which are used is based on the Kalman Filter (KF) [22] and on the Extended Kalman Filter (EKF)

[9], [14], [30], [3], [1], a KF extension which can be employed on nonlinear dynamical systems. Furthermore, such filters usually make use of simplified kinematic and dynamic models of the vehicle; such models must indeed offer a good trade-off between the accurate reproduction of reality and the demand for computational resources, in order to be used in real-time within an estimation filter without simplifying too much the physical behaviour of the AUV.

In this paper, a new motion estimation algorithm is proposed; the algorithm is based on the Unscented Kalman Filter (UKF) [20], [33], [29], and it is specifically designed for AUVs, exploiting the data acquired by the available onboard sensors, including inertial, linear velocity, acoustic and depth sensors [5], [7], [8], [23], [28]. The Unscented Kalman Filter offers a convenient trade-off between performance and computational load but, to the authors' knowledge, it has not yet been extensively used in practical underwater applications.

Particular effort has been dedicated to the development of a suitable model of the AUV, accurate enough to produce consistent results when used within a recursive estimation filter, but non too demanding in terms of required computational load.

At this initial phase of the research activity, a preliminary validation of the proposed filtering algorithm has been executed offline on the data acquired by the two Typhoon AUVs, developed and built by the Department of Industrial Engineering of the University of Florence in the framework of the Tuscany Region THESAURUS[1] project, during the FP7 European ARROWS[2] project [35] tests performed at the international workshop Breaking the Surface, held in Biograd Na Moru (Croatia) in October 2014 (Figure 1) [25]. Such experiments were performed to preliminary test the cooperative navigation between the two AUVs.

During the tests, the vehicle navigates in dead reckoning; the presented algorithm, along with the standard navigation filter of the Typhoon AUVs (which is based on the Extended Kalman Filter) are tested offline and their performance is compared, in order to evaluate the accuracy of the new navigation approach in estimating the vehicle dynamic behaviour. The obtained results are encouraging; in the near future, the proposed navigation filter will be

[1]THESAURUS project: *www.thesaurus.isti.cnr.it*

[2]ARROWS project: *www.arrowsproject.eu*

implemented on the Typhoon AUVs and will be tested online in the water during experimental campaigns.
The paper is organized as follows: Section 2 introduces the Typhoon class AUV, briefly describing its structure and the sensors it is equipped with; Section 3 illustrates the mathematical models used to describe the vehicle behaviour, including its sensors and its propulsion system; in addition, a state-space representation of the vehicle model is derived. Section 4 illustrates the recursive navigation filters, both the standard and the proposed ones; the performance comparison among the two navigation algorithms and the experimental data are finally presented in Section 5.2.

Figure 1: The Typhoon AUVs performing sea tests in Biograd Na Moru (Croatia) during BtS 2014

2. AUV description

The Typhoon class AUV is a middle-sized class AUV developed and built by the Mechatronics and Dynamic Modelling Laboratory (MDM Lab) of the Department of Industrial Engineering of the University of Florence in the

framework of the THESAURUS and the ARROWS projects.

Typhoon AUV characteristics	
Length [mm]	3600
External diameter [mm]	350
Mass [kg]	130-180 (dep. on payload)
Max speed [kn]	5-6
Max depth [m]	300
Autonomy [h]	>8

Table 1: Typhoon AUV physical data and performance

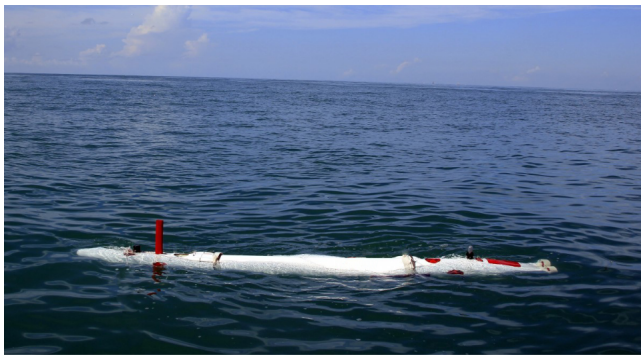

Figure 2: Typhoon AUV at sea

The physical data of the vehicle are reported in Table 1, along with the achievable performance. Currently, two versions of the Typhoon AUV have been built, named respectively TifOne and TifTu. The results presented in this paper refer to the TifOne AUV (Figure 2), communicating with TifTu during autonomous navigation (cooperative navigation).
Longitudinal, lateral and vertical motions of the Typhoon are directly controlled, along with the yaw and the pitch angles, thanks to the two main rear propellers and to the four thrusters (two vertical and two lateral), shown in Figure 3. The position of the propellers and of the thrusters on the vehicle is reported in Figure 4.
Stability against roll motion is ensured by the hydrostatic stability, i.e., the correct positioning and alignment of the centers of buoyancy and gravity.
The sensor set available for the Typhoon class AUV includes:

- Global Positioning System (GPS);

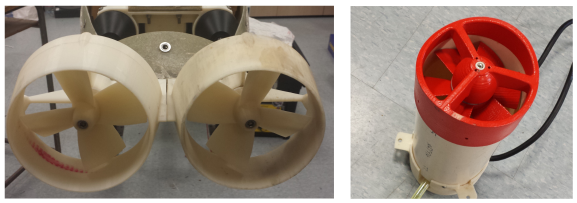

Figure 3: Typhoon AUV main propellers (left) and thrusters (right)

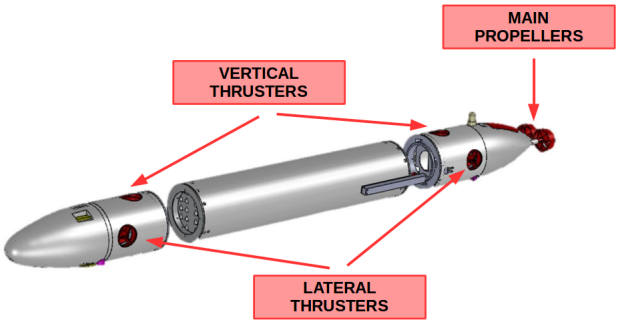

Figure 4: Typhoon AUV CAD design

- Ultra-short baseline (USBL);
- Depth sensor;
- Inertial Measurement Unit (IMU);
- Doppler Velocity Log (DVL).

The mathematical models used to describe the functioning of the available sensors are presented in Section 5.1.

3. Vehicle modelling

3.1. Kinematic and dynamic model

To conveniently describe the AUV model, two suitable reference frames are used [16], shown in Figure 5.
The fixed inertial frame $\{O^N x^N y^N z^N\}$ has its origin on the surface and its axes pointing North, East and Down (NED reference frame); the body frame $\{O^b x^b y^b z^b\}$ is centered in the center of gravity of the AUV, with the x-axis pointing in the direction of the forward motion of the vehicle, the z-axis

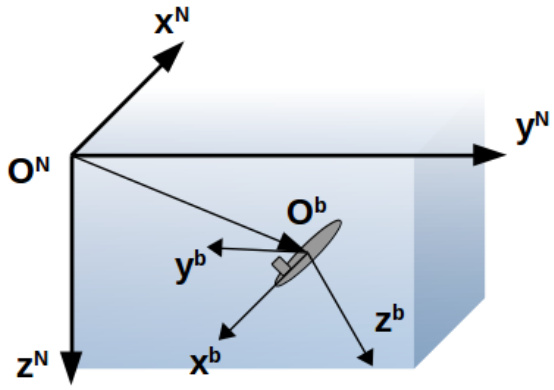

Figure 5: Inertial and body reference frames

pointing down and the y-axis completing a right-handed reference frame.
To describe the kinematic and the dynamic model of the vehicle, SNAME notation [16] has been used; hence, the model of the AUV is expressed in terms of the following vectors:

$$\begin{array}{llll} \boldsymbol{\eta} = \left[\boldsymbol{\eta}_1^T \ \boldsymbol{\eta}_2^T\right]^T & \boldsymbol{\eta}_1 = [x \ y \ z]^T & \boldsymbol{\eta}_2 = [\phi \ \theta \ \psi]^T \\ \boldsymbol{\nu} = \left[\boldsymbol{\nu}_1^T \ \boldsymbol{\nu}_2^T\right]^T & \boldsymbol{\nu}_1 = [u \ v \ w]^T & \boldsymbol{\nu}_2 = [p \ q \ r]^T \end{array} . \tag{1}$$

$\boldsymbol{\eta}$ includes the position ($\boldsymbol{\eta}_1$) and the orientation ($\boldsymbol{\eta}_2$) of the vehicle expressed in the inertial frame (note that, as regards the orientation, a triplet of Euler angles has been used; in the considered case, these angles are the roll, the pitch and the yaw angles), while $\boldsymbol{\nu}$ is composed of the linear ($\boldsymbol{\nu}_1$) and of the angular ($\boldsymbol{\nu}_2$) velocities of the AUV expressed in the body frame.
The introduced quantities are linked by the following kinematic relation:

$$\dot{\boldsymbol{\eta}} = J(\boldsymbol{\eta}_2)\boldsymbol{\nu}, \ J(\boldsymbol{\eta}_2) = \begin{bmatrix} R_b^N(\boldsymbol{\eta}_2) & 0_{3\times3} \\ 0_{3\times3} & T_b^N(\boldsymbol{\eta}_2) \end{bmatrix} , \tag{2}$$

being $R_b^N(\boldsymbol{\eta}_2)$ the rotation between the inertial and the body frame and $T_b^N(\boldsymbol{\eta}_2)$ the transformation matrix between angular velocity and the time derivatives of the chosen Euler angles.
The dynamics of the AUV is governed by the following equations [16]:

$$M\dot{\boldsymbol{\nu}} + C(\boldsymbol{\nu})\boldsymbol{\nu} + D(\boldsymbol{\nu})\boldsymbol{\nu} + \mathbf{g}(\boldsymbol{\eta}) = \boldsymbol{\tau}(\boldsymbol{\nu}, \mathbf{u}) \ . \tag{3}$$

M is the mass matrix, $C(\boldsymbol{\nu})$ and $D(\boldsymbol{\nu})$ are, respectively, the centrifugal and Coriolis matrix and the damping effects matrix, $\mathbf{g}(\boldsymbol{\eta})$ is the vector of gravitational and buoyancy effects and $\boldsymbol{\tau}(\boldsymbol{\nu}, \mathbf{u})$ is the vector of the resultant force and moment acting on the vehicle (being $\mathbf{u}$ the control inputs, i.e. the rotational speed of the motors related to the delivered thrusts [12] [27] [12] [1]).

3.2. State-space representation of the vehicle model

In order to use a recursive digital motion estimation filter (e.g. the Kalman filter), a discrete state-space representation of the model of the vehicle is needed; hence, the system must be described by a set of equations in the form:

$$\begin{cases} \mathbf{x}_k = \mathbf{f}_{k-1}(\mathbf{x}_{k-1}, \mathbf{u}_{k-1}) + \mathbf{w}_{k-1} \\ \mathbf{y}_k = \mathbf{h}_k(\mathbf{x}_k) + \mathbf{v}_k \end{cases} , \tag{4}$$

where $\mathbf{x}_k$ is the vector of state variables at the k-th instant, $\mathbf{u}_k$ and $\mathbf{y}_k$ are the inputs and the outputs of the system, and $\mathbf{w}_k$ and $\mathbf{v}_k$ are, respectively, additive process and measurement noise. The first equation in (4) is called the *system evolution equation*, while the second one is called the *measurement equation*.
In this context, the state vector has been chosen as follows:

$$\mathbf{x} = \begin{bmatrix} \boldsymbol{\eta} \\ \boldsymbol{\nu} \end{bmatrix} . \tag{5}$$

$\mathbf{x}$ is a twelve-dimensional state vector containing the kinematic quantities describing the motion of the AUV.
According to the previous sections, the time evolution of the system is defined by the following equations:

$$\begin{aligned} \dot{\mathbf{x}} = \begin{bmatrix} \dot{\boldsymbol{\eta}} \\ \dot{\boldsymbol{\nu}} \end{bmatrix} = \mathbf{F}(\mathbf{x}, \mathbf{u}) + \mathbf{w} = \\ = \begin{pmatrix} J(\boldsymbol{\eta}_2)\boldsymbol{\nu} \\ M^{-1}\left(\boldsymbol{\tau}(\boldsymbol{\nu}, \mathbf{u}) - C(\boldsymbol{\nu})\boldsymbol{\nu} - D(\boldsymbol{\nu})\boldsymbol{\nu} - \mathbf{g}(\boldsymbol{\eta})\right) \end{pmatrix} + \mathbf{w} . \end{aligned} \tag{6}$$

The model expressed in Eq. (6) has been subsequently simplified in accordance with the following considerations: since the vehicle drag along transversal directions strongly dampens the lateral and the vertical motions, considerable dynamics takes place only on the longitudinal direction (i.e. the

direction of the forward motion). This is especially true for autonomous vehicles: AUVs often possess a torpedo shape and travel along the longitudinal direction (the direction of minimal resistance) in order to save energy on board (e.g. to preserve battery charge).
In addition, a simplified model reduces the number of unknown parameters and shortens the computational time; this is especially advantageous since the model has to be used in real-time within the recursive motion estimation filter.
On the basis of these reasonable considerations, a simplified state-space model has been derived, taking into account only the longitudinal degree of freedom for what concerns the dynamics:

$$\dot{\mathbf{x}} = \begin{bmatrix} \dot{\boldsymbol{\eta}}_1 \\ \dot{\boldsymbol{\eta}}_2 \\ \dot{\boldsymbol{\nu}}_1 \\ \dot{\boldsymbol{\nu}}_2 \end{bmatrix} = \begin{pmatrix} R_b^N(\boldsymbol{\eta}_2)\boldsymbol{\nu}_1 \\ T_b^N(\boldsymbol{\eta}_2)\boldsymbol{\nu}_2 \\ \begin{bmatrix} \frac{\tau_{1x}(\boldsymbol{\nu},\mathbf{u})}{m} + F_1(\boldsymbol{\nu}) \\ 0 \\ 0 \end{bmatrix} \\ \mathbf{0}_{3\times 1} \end{pmatrix} , \tag{7}$$

being $\tau_{1x}(\cdot)$ the force acting on the vehicle x-axis [12] [27] [12] [1].
Particular attention has to be given to the equation that defines the longitudinal acceleration, denoted in Eq. (7) by:

$$\dot{\nu}_{1x} = \dot{u} = \frac{\tau_{1x}\left(\boldsymbol{\nu}, \mathbf{u}\right)}{m} + F_1(\boldsymbol{\nu}). \tag{8}$$

The expression of $F_1(\boldsymbol{\nu})$ is obtained from the complete dynamic model (3) [16], and it has been further simplified in order to reduce the number of unknown parameters:

$$F_1(\boldsymbol{\nu}) = -\frac{A_f C_u \rho \nu_{1x}^2 sgn(\nu_{1x})}{2m} , \tag{9}$$

where A_f is the frontal area of the AUV, C_u is the longitudinal drag effect coefficient and m is the mass of the vehicle.
Eq. (9) is derived under the following assumptions:

- the mass matrix is diagonal: this consideration derives from the fact that, for the Typhoon AUVs, the body reference frame is aligned with the vehicle principal axes of inertia;

- the damping matrix is diagonal: this assumption equals to neglecting the coupling between the dissipative effects, which is reasonable if velocities are not too high. In addition, with respect to the form of $D(\boldsymbol{\nu})$ given in [16], only a quadratic damping term has been considered;
- gravitational, centripetal and Coriolis effects have been neglected.

The continuous time model (7) has been subsequently discretized with a first order Euler method, in order to obtain a discrete time representation, suitable for use with a digital estimation filter. Denoting with ΔT the sampling period of the discrete time system, the following equations have been derived:

$$\begin{aligned}\begin{bmatrix}\boldsymbol{\eta}_1\\ \boldsymbol{\eta}_2\\ \boldsymbol{\nu}_1\\ \boldsymbol{\nu}_2\end{bmatrix}_k &= \mathbf{f}_{k-1}(\mathbf{x}_{k-1},\mathbf{u}_{k-1}) + \mathbf{w}_{k-1} = \\ &= \begin{pmatrix} (\boldsymbol{\eta}_1)_{k-1} + \Delta T R_b^N\left((\boldsymbol{\eta}_2)_{k-1}\right)(\boldsymbol{\nu}_1)_{k-1} \\ (\boldsymbol{\eta}_2)_{k-1} + \Delta T T_b^N\left((\boldsymbol{\eta}_2)_{k-1}\right)(\boldsymbol{\nu}_2)_{k-1} \\ \begin{bmatrix}\frac{(\tau_{1x})_{k-1}(\boldsymbol{\nu}_{k-1},\mathbf{u}_{k-1})}{m} + (F_1)_{k-1}(\boldsymbol{\nu}_{k-1})\\ 0\\ 0\end{bmatrix} \\ (\boldsymbol{\nu}_2)_{k-1}\end{pmatrix} + \mathbf{w}_{k-1}\ .\end{aligned} \tag{10}$$

As regards the measurement equation, the available quantities are the outputs of the sensors mounted on the vehicle:

$$\begin{aligned}\mathbf{y}_k = \Big[x^{meas,GPS}\ y^{meas,GPS}\ \left(\boldsymbol{\eta}_1^{meas,USBL}\right)^T \\ z^{meas}\ \left(\boldsymbol{\eta}_2^{meas}\right)^T\ \left(\boldsymbol{\nu}_1^{meas}\right)^T\ \left(\boldsymbol{\nu}_2^{meas}\right)^T\Big]_k^T\ .\end{aligned} \tag{11}$$

Hence, the measurement equation is affine: the measurement function $\mathbf{h}_k(\cdot)$ can be expressed through a matrix H_k^{meas} whose rows contain 1 or 0 elements, and vector $\mathbf{v}_k$ collects the measurement noise for each sensor introduced in Section 5.1:

$$\mathbf{y}_k = H_k^{meas}\mathbf{x}_k + \mathbf{v}_k\ . \tag{12}$$

The actual size of the matrix H_k^{meas} changes at each sampling time: since the sensors possess different working frequencies, once ΔT has been fixed the

sensors are queried for a new measurement at each sampling period, and if none is available the corresponding row of H_k^{meas} is removed.
In view of Equations (7)-(9) the state-space representation of the (simplified) model of the vehicle is highly nonlinear and non-differentiable (note, for instance, the presence of the quadratic terms or of the sign function); this implies the impossibility of using a linear filtering algorithm to estimate the state of the vehicle (such as the Kalman filter).
Particular attention must be paid to the measurement of the orientation $\boldsymbol{\eta}_2$ (see also Section 5.2 for further details) that deeply affects the performance of the navigation algorithm. In this application, a Xsens® MTI IMU sensor has been used. Such a device is able to detect little orientation variations in 3D thanks to an estimate inner owner algorithm. The algorithm used within the Xsens platform is a protected information, i.e. a proprietary algorithm exploited for orientation estimation based on raw data from accelerometers, gyroscopes and magnetometers: an example of the state of the art on this topic is [24]. The orientation angles provided by the Xsens and preprocessed through the proprietary algorithm $\boldsymbol{\eta}_2$ are then used into the navigation filter to evaluate $\boldsymbol{\eta}_2^{meas}$.
In case of highly disturbed environments, e.g. in presence of metal objects that create non-negligible magnetic noise, the navigation strategy used to guarantee a valid vehicle localization is based on two independent algorithms, respectively an orientation estimation one and a position estimation one. The former does not exploit anymore only the Xsens and the sensor fusion within a Nonlinear Complementary Filter: in order to be robust, the authors integrated in the system also a single-axis Fiber Optic Gyroscope (FOG) and developed an innovative algorithm in the underwater field to have a reliable orientation estimation [34]. Also in this circumstance, the orientation angles provided by the Xsens and preprocessed through the new algorithm $\boldsymbol{\eta}_2$ are then used into the navigation filter to evaluate $\boldsymbol{\eta}_2^{meas}$.

4. Navigation filter

This Section introduces the navigation filters used to estimate the state vector of the system, the performances of which will be compared in Section 5.2.
The nonlinearity of the system evolution model (10) implies that a linear filter cannot be used to estimate the system state. Hence, two nonlinear

filters have been employed, namely the Extended Kalman Filter (EKF) and the Unscented Kalman Filter (UKF) [22], [9], [20], [33], [29].
Given the vehicle model expressed in a suitable state-space representation (4), the standard navigation filter is based on the EKF [9], [14], [30], [3], [1]; it is composed of the prediction/correction scheme shown in Alg. 1.

Function *EKF algorithm*
  Step *EKF prediction*
    Data: $\hat{\mathbf{x}}_{k-1|k-1}$, $P_{k-1|k-1}$, $\mathbf{f}_{k-1}(\cdot)$
    Result: $\hat{\mathbf{x}}_{k|k-1}$, $P_{k|k-1}$
    $F_{k-1} = \left.\frac{\partial \mathbf{f}_{k-1}}{\partial \mathbf{x}}\right|_{\hat{\mathbf{x}}_{k-1|k-1}, \mathbf{u}_{k-1}}$;
    $\hat{\mathbf{x}}_{k|k-1} = \mathbf{f}_{k-1}(\hat{\mathbf{x}}_{k-1|k-1})$;
    $P_{k|k-1} = F_{k-1} P_{k-1|k-1} F_{k-1}^T + Q_{k-1}$;
  end
  Step *EKF correction*
    Data: $\hat{\mathbf{x}}_{k|k-1}$, $P_{k|k-1}$, $\mathbf{h}_k(\cdot)$
    Result: $\hat{\mathbf{x}}_{k|k}$, $P_{k|k}$
    $H_k = \left.\frac{\partial \mathbf{h}_k}{\partial \mathbf{x}}\right|_{\hat{\mathbf{x}}_{k|k-1}}$;
    $S_k = R_k + H_k P_{k|k-1} H_k^T$;
    $L_k = P_{k|k-1} H_k^T S_k^{-1}$;
    $\mathbf{e}_k = \mathbf{y}_k - \mathbf{h}_k\left(\hat{\mathbf{x}}_{k|k-1}\right)$;
    $\hat{\mathbf{x}}_{k|k} = \hat{\mathbf{x}}_{k|k-1} + L_k \mathbf{e}_k$;
    $P_{k|k} = P_{k|k-1} - L_k S_k L_k^T$;
  end
end

Algorithm 1: EKF algorithm

In Alg. 1, $\hat{\cdot}$ denotes an estimate, P is the state covariance, and Q and R are the covariance matrices of process and measurement noise, assumed as zero mean stationary white noises with zero cross-correlation. The state is recursively estimated starting from an initial guess $\left(\hat{\mathbf{x}}_{0|0},\ P_{0|0}\right)$.
While the EKF offers an easy and lightweight implementation, it suffers from the need of a good initial estimation and requires the explicit expression of the derivatives of the system evolution and of the measurements functions.
An alternative estimation technique is the UKF [20], [33]. The filter dynamics is not propagated through linearization (as the EKF), but using a

deterministic sampling technique known as the Unscented Transform (UT). The UT allows to compute the mean and the covariance matrix of a random variable (r.v.) which undergoes a generic nonlinear transformation by propagating a minimum set of its samples and exploiting the knowledge of the mean and of the covariance of the starting variable.
Let $\mathbf{a} \in \mathbb{R}^{n_a}$ be a r.v. with mean $\bar{\mathbf{a}}$ and covariance P_a, and let $\mathbf{b} = \mathbf{g}(\mathbf{a}) \in \mathbb{R}^{n_b}$ denote the r.v. obtained by propagating $\mathbf{a}$ through the nonlinear function $\mathbf{g}(\cdot) : \mathbb{R}^{n_a} \rightarrow \mathbb{R}^{n_b}$. Then, the Unscented Transform of $\mathbf{a}$ propagated through $\mathbf{g}(\cdot)$, denoted with $UT(\bar{\mathbf{a}}, P_a, \mathbf{g}(\cdot))$, is composed of the following steps:

- generate $2n_a+1$ samples (n_a is the minimum necessary number of samples) called the σ-points Σ_a, each one with the dimension of $\mathbf{a}$, exploiting the knowledge of $\bar{\mathbf{a}}$ and of P_a. The σ-points are usually chosen as symmetric with respect to the average value $\bar{\mathbf{a}}$, i.e.:

$$\Sigma_a = [\cdots \ \bar{\mathbf{a}} \ \cdots] + \omega_\sigma \left[\mathbf{0}_{n_a \times 1} \ \Gamma_a \ -\Gamma_a\right] \ ,$$

  where Γ_a is such that $P_a = \Gamma_a \Gamma_a^T$ (e.g. the matrix square root or the Cholesky factor) and ω_σ is a weight factor;

- propagate the σ-points through $\mathbf{g}(\cdot)$:

$$\mathcal{G} = \mathbf{g}(\Sigma_a) \in \mathbb{R}^{n_b \times 2n_a+1} \ ;$$

- compute the mean $\bar{\mathbf{b}}$, the covariance matrix P_b and the cross-covariance P_{ab} from the σ-points of the propagated r.v.:

$$\bar{\mathbf{b}} = \mathcal{G}\boldsymbol{\omega}_m$$

$$P_b = \mathcal{G}\Omega_c\mathcal{G}^T$$

$$P_{ab} = \Sigma_a\Omega_c\mathcal{G}^T$$

  for suitable weights $\boldsymbol{\omega}_m \in \mathbb{R}^{2n_a+1}$ and $\Omega_c \in \mathbb{R}^{2n_a+1 \times 2n_a+1}$.

It is easy to note that the result of the Unscented Transform strongly depends on the choice of the weights ω_σ, $\boldsymbol{\omega}_m$ and Ω_c: in the considered case study, they are computed as in Alg. 2.
In Alg. 2 I is the identity matrix, $diag\{\mathbf{v}\}$ is a diagonal matrix whose diagonal elements are the components of vector $\mathbf{v}$, and $\otimes$ is the Kronecker product. Moment matching properties and performance improvements associated with

Function *UKF weights computation*

Data: α, β, γ

Result: ω_σ, $\boldsymbol{\omega}_m$, Ω_c

$\omega_\sigma = \sqrt{\alpha^2(n_a+\gamma)}$;

$\lambda = \alpha^2(n_a+\gamma) - n_a$;

$\boldsymbol{\omega}_m(0) = \lambda(n_a+\lambda)^{-1}$;

$\boldsymbol{\omega}_c(0) = \lambda(n_a+\lambda)^{-1} + (1-\alpha^2+\beta)$;

$\boldsymbol{\omega}_m(i), \boldsymbol{\omega}_c(i) = [2(n_a+\lambda)]^{-1},\ i = 1, ..., 2n_a$;

$\Delta = (I_{2n_a+1} - \mathbf{1}_{1\times 2n_a+1} \otimes \boldsymbol{\omega}_m)$;

$\Xi = diag\{\boldsymbol{\omega}_c\}$;

$\Omega_c = \Delta\Xi\Delta^T$;

end

Algorithm 2: UKF weights computation

Function *UKF algorithm*

Step *UKF prediction*

Data: $\hat{\mathbf{x}}_{k-1|k-1}$, $P_{k-1|k-1}$, $\mathbf{f}_{k-1}(\cdot)$

Result: $\hat{\mathbf{x}}_{k|k-1}$, $P_{k|k-1}$

$(\hat{\mathbf{x}}_{k|k-1}, \bar{P}_{k|k-1}) = UT(\hat{\mathbf{x}}_{k-1|k-1}, P_{k-1|k-1}, \mathbf{f}_{k-1}(\cdot))$;

$P_{k|k-1} = \bar{P}_{k|k-1} + Q_{k-1}$;

end

Step *UKF correction*

Data: $\hat{\mathbf{x}}_{k|k-1}$, $P_{k|k-1}$, $\mathbf{h}_k(\cdot)$

Result: $\hat{\mathbf{x}}_{k|k}$, $P_{k|k}$

$(\hat{\mathbf{y}}_{k|k-1}, \bar{S}_k, P_k^{xy}) = UT(\hat{\mathbf{x}}_{k|k-1}, P_{k|k-1}, \mathbf{h}_k(\cdot))$;

$S_k = R_k + \bar{S}_k$;

$L_k = P_k^{xy} S_k^{-1}$;

$\mathbf{e}_k = \mathbf{y}_k - \hat{\mathbf{y}}_{k|k-1}$;

$\hat{\mathbf{x}}_{k|k} = \hat{\mathbf{x}}_{k|k-1} + L_k\mathbf{e}_k$;

$P_{k|k} = P_{k|k-1} - L_k S_k L_k^T$;

end

end

Algorithm 3: UKF algorithm

the choice of the parameters α, β and γ are discussed in [33], [21].
The UT is used within the UKF as shown in Alg. 3, with the same notation of Alg. 1.

The main advantage associated with the use of the UKF is that it does not require the computation of derivatives, hence it can be used with models that include discontinuous functions, always present in the case of AUVs models (e.g. the propulsion system model); in addition, it offers a good trade-off between estimation accuracy and computational efficiency. However, even if the computing units which are nowadays available on AUVs could afford the load required by the UKF, to the authors' knowledge very few reports of its use in the field of underwater robotics can be found in literature [6], [17].

5. Results

In this chapter the main results obtained by comparing the considered navigation algorithms will be presented. Firstly, the main sensors the AUV is equipped with will be briefly described in terms of modelling and specifications. Subsequently, the comparison between the navigation algorithms will analyzed in detail.

5.1. Sensor modelling

This Section deals with the modelling of the sensors mounted on the Typhoon class AUVs and presented in Section 2, illustrating the mathematical models used to describe their functioning.

GPS Adafruit module; working frequency 10Hz. The GPS provides the coordinates of the vehicle, given as latitude and longitude. In order to exploit such measurements within the navigation filter it is necessary to operate a preliminary conversion to determine the corresponding inertial frame coordinates. Standard functions are available to comply with this purpose (e.g. [31]). Denoting with $\boldsymbol{f}_{GPS}(\cdot)$ the general conversion function, the characteristic equation of the sensor can be expressed as:

$$\begin{bmatrix} \eta_{1x}^{meas,GPS} \\ \eta_{1y}^{meas,GPS} \end{bmatrix} = \begin{bmatrix} x^{meas,GPS} \\ y^{meas,GPS} \end{bmatrix} = \boldsymbol{f}_{GPS}\left(\boldsymbol{ll}^{meas} + \boldsymbol{\delta}_{ll}, \boldsymbol{O}^{N}\right) \ , \tag{13}$$

where $\boldsymbol{ll}^{meas}$ is the vector containing the GPS latitude and longitude measurements. Note that, because of the nonlinearity of the transformation $\boldsymbol{f}_{GPS}(\cdot)$, the resulting measurement noise is not characterized by the same spectral properties of the noise $\boldsymbol{\delta}_{ll}$ affecting the raw GPS data;

Evologics® S2CR 18/34 USBL; working frequency 0.2Hz. The USBL transducer measures the position of a transmitting compatible modem with respect to itself [23], [28]:

$$\boldsymbol{\eta}_1^{meas,USBL} = \boldsymbol{\eta}_1 + \boldsymbol{\delta}_{\boldsymbol{\eta}_1}^{USBL} \ , \tag{14}$$

with added $\boldsymbol{\delta}_{\boldsymbol{\eta}_1}^{USBL}$ measurement noise;

STS® DTM Digital Pressure Transmitter (DPT); working frequency 10Hz. This sensor measures the local pressure following the equation:

$$p^{meas} = p^{loc} + b_p + \delta_p \ , \tag{15}$$

being p^{loc} the local pressure, and b_p and δ_p bias and measurement noise. The pressure measurement is then converted into a depth measure according to the basic hydrostatic equation:

$$p^{meas} - p^{atm} = \rho g z^{meas} \ , \tag{16}$$

where p^{atm} is the local atmospheric pressure (measured by the DPT during the initialization phase), ρ is the water density and g is the norm of the gravitational acceleration; hence, the measured depth can be expressed as:

$$\eta_{1z}^{meas} = z^{meas} = z + \delta_z \ . \tag{17}$$

Note that the DPT added bias cancels in the subtraction (16).

Xsens® MTI IMU; working frequency 100Hz. The mounted Inertial Measurement Unit is composed of a three-axis accelerometer, a three-axis gyroscope and a three-axis magnetometer. Each sensor has been modelled separately:

- *Accelerometer: measures the proper acceleration of the vehicle, biased by the gravitational acceleration $\boldsymbol{g}_E$. The measure is expressed in the body frame as follows:*

$$\boldsymbol{a}^{meas} = \left(R_b^N\right)^T (\ddot{\boldsymbol{\eta}}_1 - \boldsymbol{g}_E) + \boldsymbol{b}_a + \boldsymbol{\delta}_a \ , \tag{18}$$

  where $\boldsymbol{b}_a$ and $\boldsymbol{\delta}_a$ are, respectively, added bias and measurement noise;

- *Gyroscope: this sensor measures the angular velocity of the AUV in the body frame according to the following model:*

$$\boldsymbol{\nu}_2^{meas} = \boldsymbol{\nu}_2 + \boldsymbol{b}_{\boldsymbol{\nu}_2} + \boldsymbol{\delta}_{\boldsymbol{\nu}_2} \ . \tag{19}$$

In addition to the measurement noise $\boldsymbol{\delta}_{\boldsymbol{\nu}_2}$, a bias $\mathbf{b}_{\boldsymbol{\nu}_2}$ is present; in contrast with the accelerometer bias (which is constant), the gyroscope bias considerably varies over time; hence, it has to be estimated and compensated in real-time;

- *Magnetometer: measures the local magnetic field around the sensor, expressed in the body frame:*

$$\boldsymbol{m}^{meas} = W \left(R_b^N\right)^T \boldsymbol{H}^N + \boldsymbol{H}_d + \boldsymbol{\delta}_m \ . \tag{20}$$

The measure of the Earth's magnetic field $\boldsymbol{H}^N$ is affected by the measurement noise $\boldsymbol{\delta}_m$ and by the effects of magnetic disturbances, modelled as an additional bias $\boldsymbol{H}_d$ (Hard Iron effect) and by a matrix W (Soft Iron, scale factor and misalignment errors) [32], which have to be compensated before the employment of the sensor.

The raw data coming from the IMU have been fused using the nonlinear complementary filter proposed by Mahony et al. in 2008 [24], to obtain a reliable estimation of the orientation of the vehicle:

$$\boldsymbol{\eta}_2^{meas} = \boldsymbol{\eta}_2 + \boldsymbol{\delta}_{\boldsymbol{\eta}_2} \ , \tag{21}$$

being $\boldsymbol{\delta}_{\boldsymbol{\eta}_2}$ measurement noise.

Teledyne Explorer® Doppler Velocity Log (DVL); working frequency 10Hz. This sensor measures the linear velocity of the vehicle [28]; the following model has been used:

$$\boldsymbol{\nu}_1^{meas} = \boldsymbol{\nu}_1 + \mathbf{b}_{\boldsymbol{\nu}_1} + \boldsymbol{\delta}_{\boldsymbol{\nu}_1} \ , \tag{22}$$

where the measured quantity $\boldsymbol{\nu}_1^{meas}$ is the sum of the true value $\boldsymbol{\nu}_1$, of the bias error $\mathbf{b}_{\boldsymbol{\nu}_1}$ and of the measurement noise $\boldsymbol{\delta}_{\boldsymbol{\nu}_1}$.
The sensor set each AUV is equipped with is slightly different; see Table 2 for the list of the devices mounted on each vehicle.

5.2. Comparison between the navigation algorithms

The proposed navigation filter has been experimentally validated exploiting the data acquired during suitable sea tests held in Biograd Na Moru (Croatia) in October 2014 during the international workshop Breaking the Surface (BtS 2014, Figure 1) [25] in the framework of the FP7 European ARROWS project.

Typhoon class AUV sensor sets		
Sensor	**TifOne**	**TifTu**
GPS	✓	✓
USBL	Localizable Modem	Localizing Transducer
Depth Sensor	✓	✓
IMU	✓	✓
DVL	✓	✗

Table 2: TifOne and TifTu sensor sets

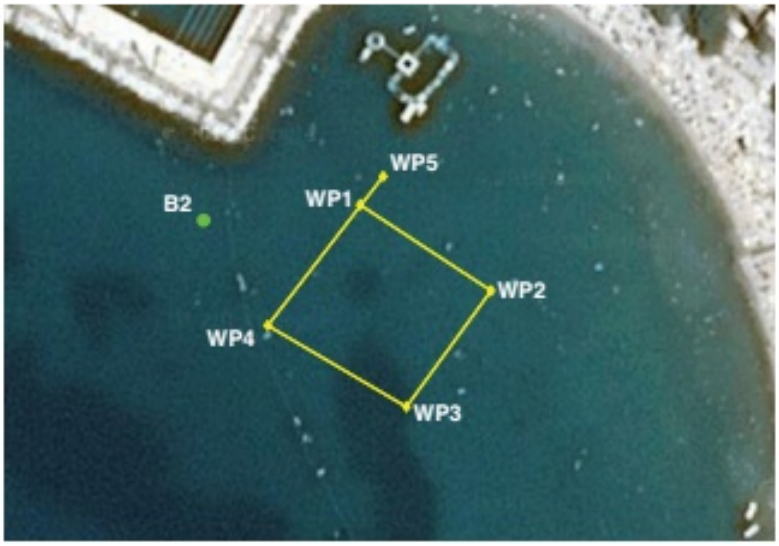

Figure 6: Layout of the autonomous mission: square-shaped path with vertices placed in WP1, WP2, WP3, WP4 and WP5

Waypoint Name	**Latitude** [°]	**Longitude** [°]	**Depth** [m]
WP1	43.932571° N	15.445007° E	0.0 m
WP2	43.932358° N	15.445458° E	0.0 m
WP3	43.932071° N	15.445167° E	0.0 m
WP4	43.932272° N	15.444689° E	1.5 m
WP5	43.932642° N	15.445087° E	1.5 m

Table 3: Waypoints for TifOne mission

The Typhoon AUV TifOne, navigating in dead reckoning, is required to perform an autonomous mission consisting in navigating through five waypoints which form the square-shaped path shown in Figure 6.
The path through the first three waypoints WP1-WP3 has to be followed on surface, while the desired depth for the last two legs of the square is of 1.5 m. The total path measures 179 m, and it is followed clockwise; the AUV stops to execute each 90° turn and to submerge, while the desired speed for the legs is constant and fixed at 0.6 or 0.8 m/s (depending on the test). Table 3 summarizes the coordinates of the five waypoints; the buoy B2 visible in Figure 6 represents the USBL transducer mounted on TifTu, which is moored at the coordinates 43.932533° N, 15.444468° E. The demonstration held at BtS 2014 is a preliminary test of cooperative navigation between these two AUVs, as the position of TifOne is measured through the USBL mounted on TifTu. Localization data are made available to TifOne through acoustic communication.
The validation of the proposed UKF-based navigation filter has been executed offline: the behaviour of the filter has been validated in a Matlab® environment using the data acquired by the sensors mounted on the vehicle during the execution of the autonomous mission. The goal of these simulations is to compare the performances of the proposed filter to the ones of the standard EKF-based navigation filter, comparing their outputs to the corresponding quantities measured by the sensors; furthermore, different sensor configurations have been analysed, and the effects of the presence (or the absence) of particular sensors on the output of the filters are shown. In particular, the following sensor combinations have been considered:

- Configuration I: AUV equipped with IMU and depth sensor, exploiting the GPS signal while on surface;
- Configuration II: AUV equipped with IMU, depth sensor and DVL, exploiting the GPS signal while on surface;
- Configuration III: AUV equipped with IMU, depth sensor and DVL, exploiting the GPS signal while on surface and the USBL while underwater.

Several tests have been conducted on the field during a two days timespan; the results here proposed refer to two tests assumed as case study.
Figures 7-9 show the position (x-axis and y-axis) estimated by the two filters

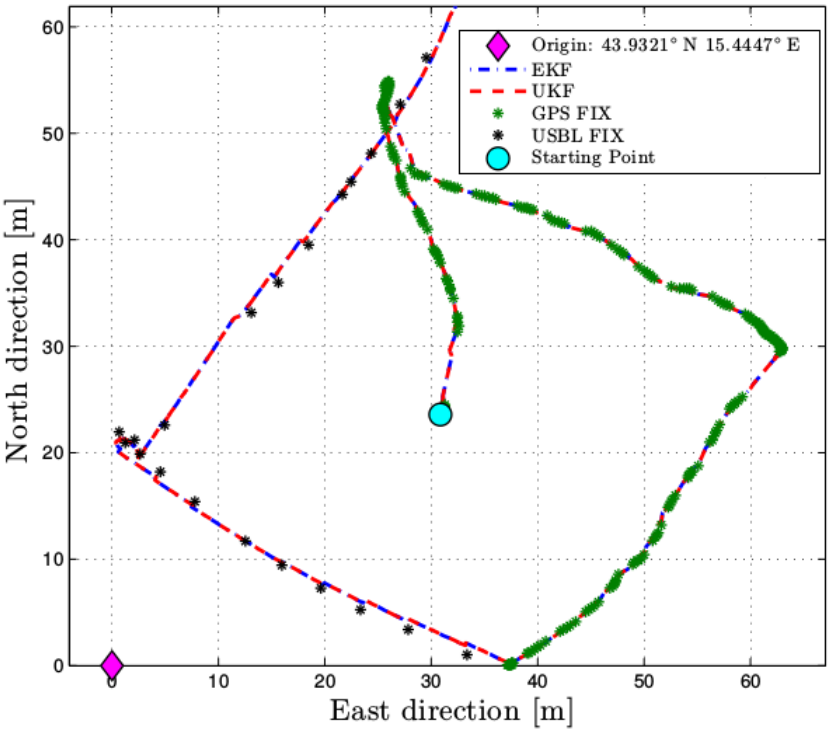

Figure 7: Test 1: position estimation comparison between the two navigation filters in Configuration III

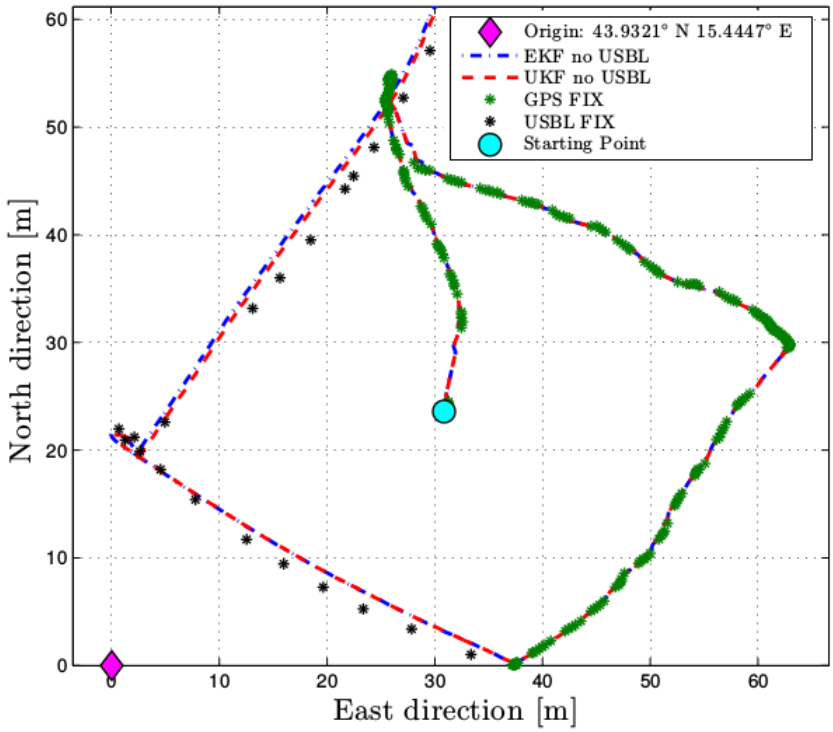

Figure 8: Test 1: position estimation comparison between the two navigation filters in Configuration II

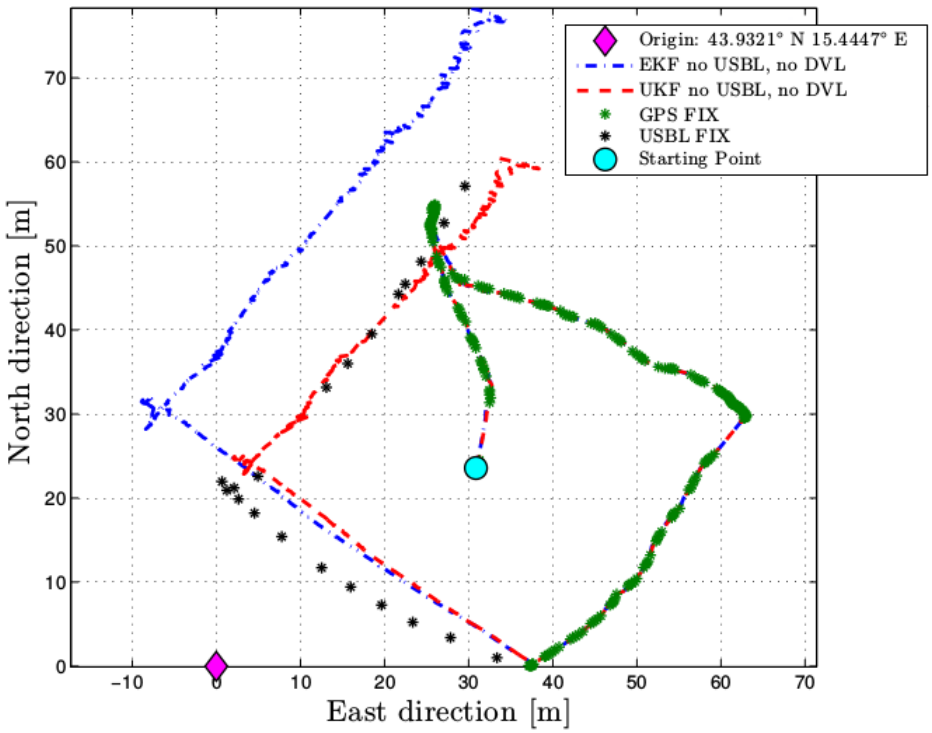

Figure 9: Test 1: position estimation comparison between the two navigation filters in Configuration I

with different sensor configurations during the first test; as expected, the performance of both the EKF and the UKF deteriorates as the number of available sensors is reduced.
For what concerns the comparison between the two strategies, it is easily visible that both offer similar performance while the vehicle navigates on surface, regardless of the sensor configuration: this is because the GPS signal is always available and its fixes are predominant in the correction step of the filters.
A relevant difference in the behaviour of the two navigation filters is shown when the AUV navigates underwater: in this case, the contributions given by the USBL and by the DVL become fundamental to achieve limited error estimates. When the available set of sensors is reduced, the performance gap between the two navigation strategies becomes larger, showing the superiority of the proposed UKF-based filter compared to the standard EKF-based solution.
To better support this thesis, Figure 10 reports the distance (expressed in metres) between $\left[\eta_{1x}^{USBL}\ \eta_{1y}^{USBL}\right]^T$, which contains the x-axis and y-axis position of the USBL fixes, and $\left[\eta_{1x}^{EKF}\ \eta_{1y}^{EKF}\right]^T$, $\left[\eta_{1x}^{UKF}\ \eta_{1y}^{UKF}\right]^T$, evaluated at the time instants where each USBL fix is acquired: in Configuration III the estimation error is almost the same for both filters; in Configuration II the UKF behaves slightly better, while in Configuration I, with the reduced set of sensor, the accuracy improvement offered by the proposed filter is relevant. It is clearly visible that, when the DVL integration is not available, the EKF shows a position error of more than 10-15 m, while the error obtained with the proposed UKF-based strategy remains much lower (less than 6 m). *More particularly, the UKF-based navigation algorithm turns out to be more robust than the EKF-based one especially when the prediction part of the filter becomes predominant if compared to the correction part. In other words, the new approach provides better results if reduced sets of sensors are employed and reduced measurements are available.*

In particular, considering Configuration III, the limited error (<2 m) between the estimated position and the USBL fixes indicates that the vehicle model used within the filter is consistent with the AUV physical behaviour. *For the sake of completeness, in Figure 14 the measured and estimated vehicle orientations (roll, pitch and yaw) are reported for sensor set Configuration I (test 1). Only the results related to Configuration I are reported because this is the most critical one. As it can be seen, the behaviour of the two navigation*

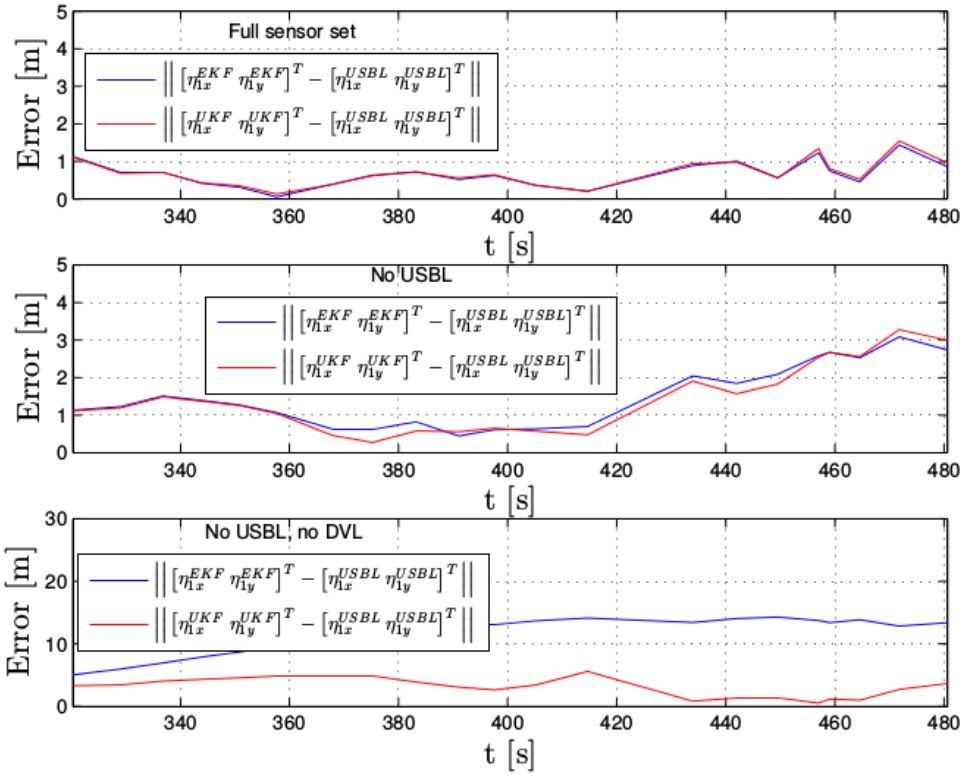

Figure 10: Test 1: position error between the output of the filters and the USBL fixes during underwater navigation for Configurations I, II and III

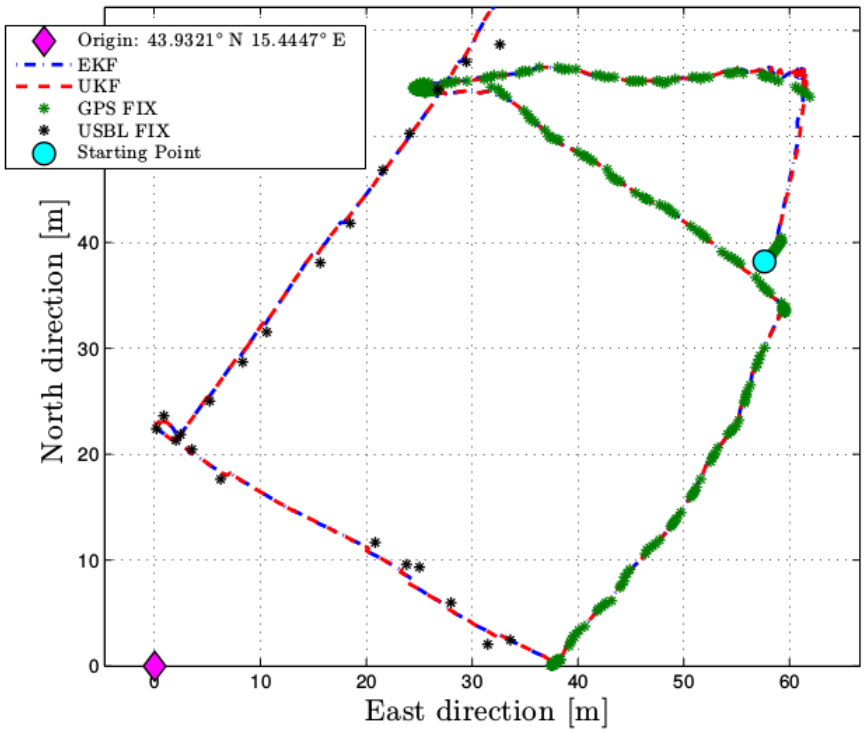

Figure 11: Test 2: position estimation comparison between the two navigation filters in Configuration III

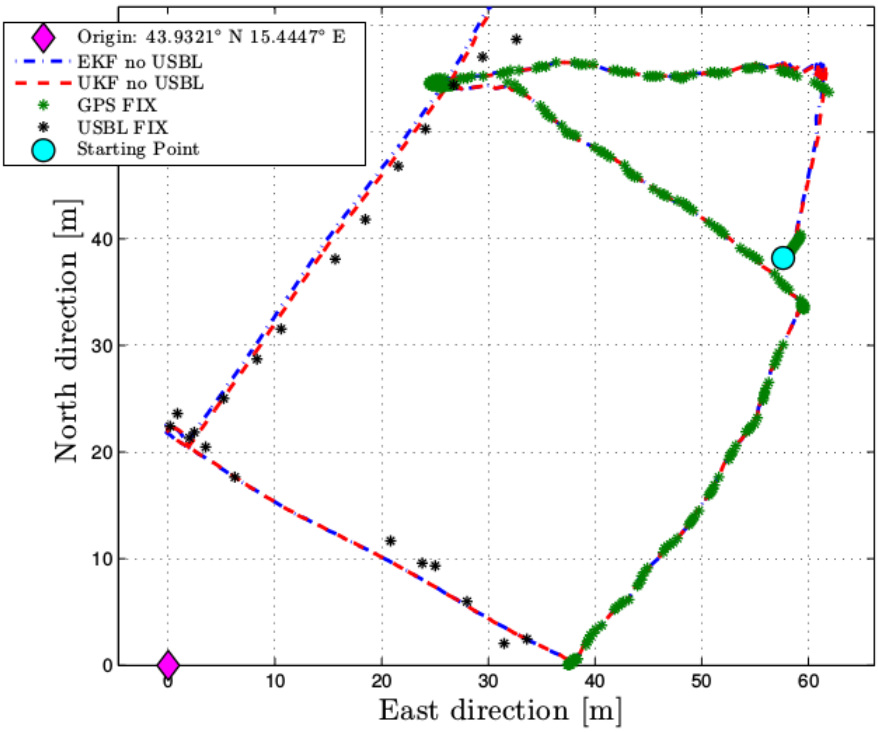

Figure 12: Test 2: position estimation comparison between the two navigation filters in Configuration II

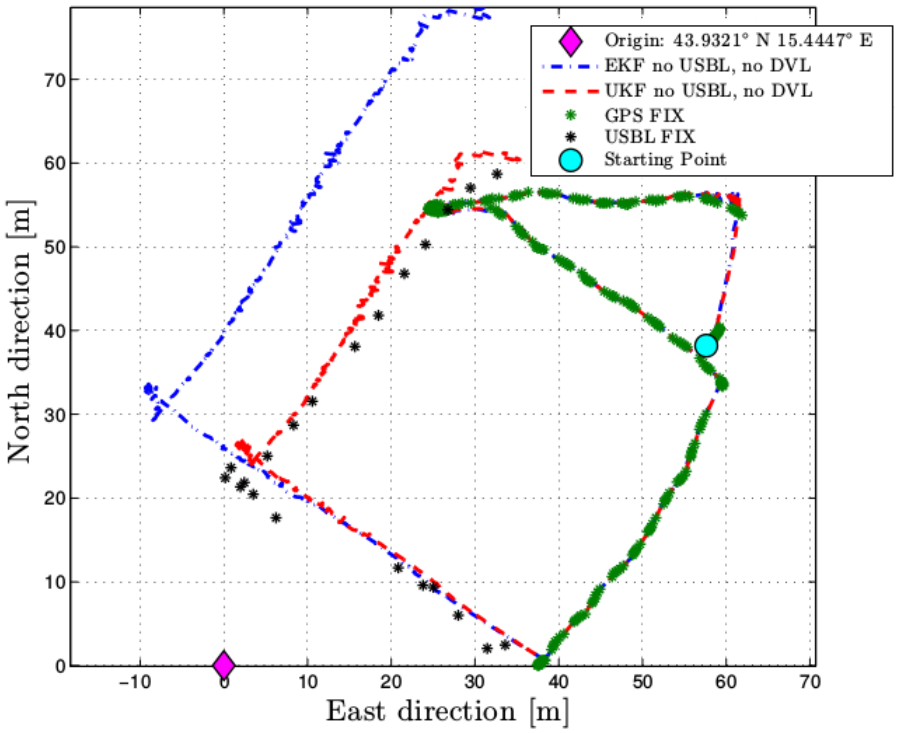

Figure 13: Test 2: position estimation comparison between the two navigation filters in Configuration I

filters is quite the same in terms of orientations, mainly due to the accuracy of IMU sensors.

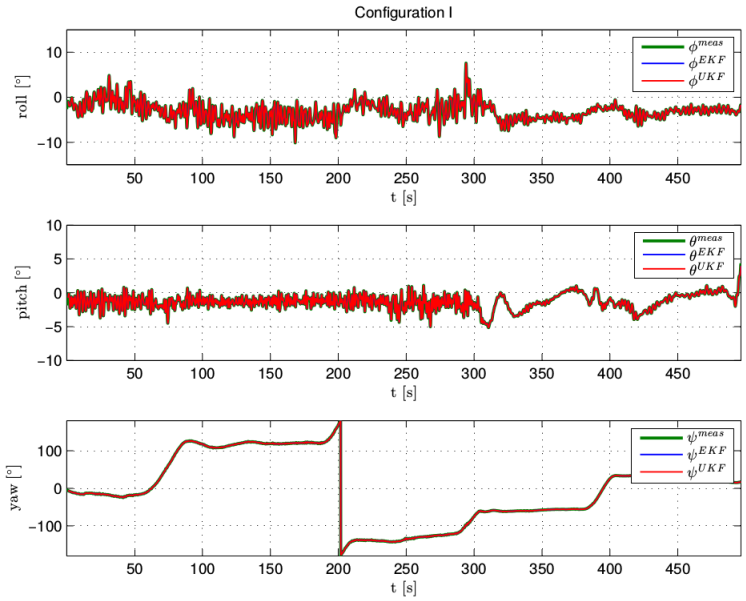

Figure 14: Test 1: orientation estimation comparison between the two navigation filters in Configuration I

The same results are reported for the second test: Figures 11-13 show the performances of the two solutions with different sensor sets, while Figure 15 compares the estimated position with the USBL fixes.

Analogously, in Figure 16 the measured and estimated vehicle orientations (roll, pitch and yaw) are reported for sensor set Configuration I (test 2). Also in this case, the accuracy of the two navigation filters in terms of orientations turns out to be very similar.

The two tests reported (along with the others performed and the results of which are not shown here) allow to establish the repeatability of the behaviour of the navigation filters. *As in the previous case, the UKF-based navigation algorithm turns out to be more robust than the EKF-based one especially when reduced sets of sensors are employed and reduced measurements are available. Under this circumstance, the prediction part of the filter becomes predominant if compared to the correction part. Furthermore, such improvement is also due to the intrinsic difficulties faced by the EKF in the*

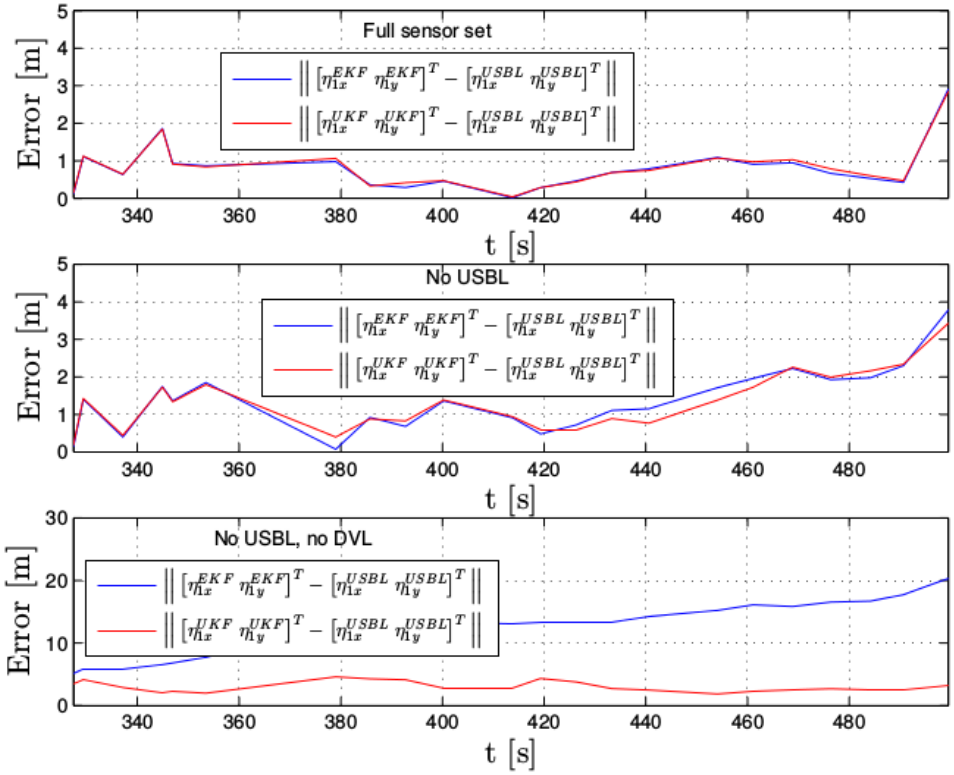

Figure 15: Test 2: position error between the output of the filters and the USBL fixes during underwater navigation for Configurations I, II, III

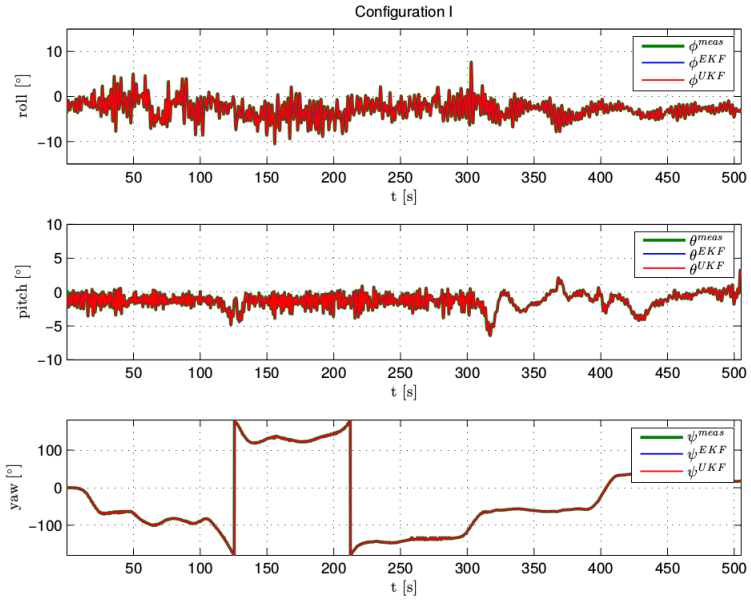

Figure 16: Test 2: orientation estimation comparison between the two navigation filters in Configuration I

case of nonlinear and/or discontinuous systems. For these reasons, the UKF-based approach turns out to be promising to assure lower estimation errors in complex navigation and cooperation tasks.

6. Conclusion

In this paper the authors presented an innovative navigation system especially designed for AUVs. This strategy exploits a new navigation algorithm based on the Unscented Kalman Filter (UKF). The innovative approach allows to achieve a very effective trade-off between accuracy and computational load. The proposed navigation strategy has been experimentally validated offline exploiting real sensor data acquired by TifOne and TifTu, the two Typhoon class AUVs developed and built by the MDM Lab of the University of Florence, during the FP7 European ARROWS project tests performed at the international workshop Breaking the Surface 2014. These tests constitute a preliminary experiment of cooperative navigation between the two vehicles. The achieved results are promising, showing encouraging improvements in estimating the vehicle dynamics with respect to the standard navigation system, based on the Extended Kalman Filter (EKF), especially in the case of

discontinuous and strongly nonlinear systems.
Important further developments are scheduled for the future. Firstly, the new UKF-based navigation filter will be simulated online within a complete model of vehicle and environment. Subsequently, the innovative system will be implemented on the Typhoon AUV and tested online in the water. This way, the performance of the new approach in terms of accuracy will be carefully investigated in different scenarios.

Acknowledgements

This work has been partially supported by the Italian THESAURUS project (funded by PAR FAS Regione Toscana, Linea di Azione 1.1.a.3) and by the European ARROWS project, that has received funding from the European Union's Seventh Framework Programme for research, technological development and demonstration under grant agreement no 308724. The authors would like to thank the Organizers of the international workshop Breaking the Surface 2014 and, in particular, Prof. Zoran Vukić and Prof. Nikola Mišković from the Laboratory for Underwater Systems and Technologies (LABUST) of the Faculty of Electrical Engineering and Computing of the Zagreb University (Croatia).

References

[1] Allotta B., Bartolini F., Costanzi R., Monni N., Pugi L., Ridolfi A., *Preliminary design and fast prototyping of an autonomous underwater vehicle propulsion system*, in Proceedings of the Institution of Mechanical Engineers, Part M: Journal of Engineering for the Maritime Environment, Jan. 27 (2014); DOI 10.1177/1475090213514040.

[2] Allotta B., Costanzi R., Meli E., Pugi L., Ridolfi A., Vettori G., *Cooperative localization of a team of AUVs by a tetrahedral configuration*, Robotics and Autonomous Systems, Vol. 62, N. 8, pp. 1228-1237, Aug. (2014).

[3] Allotta B., Costanzi R., Monni N., Pugi L., Ridolfi A., and Vettori G., *Design and Simulation of an Autonomous Underwater Vehicle*, in Proceedings of the European Congress on Computational Methods in Applied Sciences and Engineering (ECCOMAS), Vienna, Austria, Sept. 10-14 (2012).

[4] Antonelli G., *Underwater Robots*, Springer Tracts in Advanced Robotics, Springer-Verlag, 2nd edition, Heidelberg (2006).

[5] Arrichiello F., Antonelli G., Aguiar A.P., Pascoal A., *Observability Metric for the Relative Localization of AUVs Based on Range and Depth Measurements*, IEEE/RSJ International Conference on Intelligent Robots and Systems (IROS), San Francisco, CA, USA (2011).

[6] Barisic M., Vasilijevic A., Nad D., *Sigma-Point Unscented Kalman Filter Used For AUV Navigation*, 20th Mediterranean Conference on Control & Automation (MED), Barcelona, Spain, Jul. 3-6 (2012).

[7] Bahr A. Leonard J., Fallon M., *Cooperative Localization for Autonomous Underwater Vehicles* The International Journal of Robotics Research, Vol. 28, pp. 714-728 (2009).

[8] Bhar A., Walter M., Leonard J., *Consistent Cooperative Localization* in Proceedings of the IEEE International Conference of Robotics and Automation (ICRA), Kobe, JPN (2009).

[9] Bar-Shalom Y., Li X.R., Kirubarajan T., *Estimation with Applications to Tracking and Navigation: Theory Algorithms and Software*, Wiley, Jul. (2001).

[10] Breivik M., Fossen T. I., *Giudance-Based Path Following for Autonomous Underwater Vehicles*, in Proceedings of the OCEANS'05, Washington D.C., USA (2005).

[11] Caffaz A., Caiti A., Casalino G., Turetta A., *The Hybrid Glider/AUV Folaga*, IEEE Robotics and Automation Magazine, Vol. 17, pp. 31-44, Mar. (2010).

[12] Carlton J.S., *Marine Propellers and Propulsion*, 2nd ed., Elsevier (2007).

[13] Cheng X., Shu H., Liang Q., Du D.H.-C., *Silent Positioning in Underwater Acoustic Sensor Networks*, IEEE Trans. on Vehicular Technology, Vol. 57, N. 3, May (2008).

[14] Evensen G., editor, *Data Assimilation*, Springer Verlag, Heidelberg, Germany (2009).

[15] Fjellstad O.-E., Fossen T.I., *Position and Attitude Tracking of AUV's: A Quaternion Feedback Approach*, IEEE Journal of Oceanic Engineering, Vol. 19, N. 4, pp. 512-518, Oct. (1994).

[16] Fossen T. I., *Guidance and Control of Ocean Vehicles*, 1st ed., John Wiley & Sons, Chichester UK (1994).

[17] Hajiyev C., Ata M., Dinc M., Soken H.E., *Fault tolerant estimation of autonomous underwater vehicle dynamics via robust UKF*, 13th International Carpathian Control Conference, pp. 203-208, May 28-31 (2012).

[18] Siciliano B., Khatib O., *Handbook of Robotics*, Springer Handbooks, Napoli and Stanford (2008).

[19] Isbitiren G., Akan O.B., *Three-Dimensional Underwater Tracking With Acoustic Sensor Networks*, IEEE Trans. on Vehicular Technology, Vol. 60, N. 8, Oct. (2011).

[20] Julier S.J., Uhlmann J.K., *A New extension of the Kalman Filter to Nonlinear Systems*, in Proceedings of the SPIE Signal Processing, Sensor Fusion and Target Recognition VI Conference, Vol. 3068, Jul. 28 (1997).

[21] Julier S.J., Uhlmann J.K., *Unscented Filtering and Nonlinear Estimation*, in Proceedings of the IEEE, pp. 401-422 (2004).

[22] Kalman R.E., *A New Approach to Linear Filtering and Prediction Problems*, Trans. of the ASME Journal of Basic Engineering, Vol. 82, Series D, pp 35-45 (1960).

[23] Larsen M., *Synthetic Long Baseline Navigation of Underwater Vehicles*, in Proceedings of MTS/IEEE OCEANS 2000, Providence, RI, USA (2000).

[24] Mahony R.E., Hamel T., Pflimlin J.M., *Nonlinear Complementary Filters on the Special Orthogonal Group*, IEEE Trans. on Automatic Control, Vol. 53, N. 5, pp 1203-1218 (2008).

[25] Official website of the international workshop Breaking the Surface: *http://bts.fer.hr*

[26] Petres C., Pailhas Y., Patron P., Petillot Y., Evans J., Lane D., *Path planning for autonomous underwater vehicles*, IEEE Trans. on Robotics, Vol. 23, pp. 331-341 (2007).

[27] Pivano L., Johansen T.A., Smogeli Ø.N., *A Four-Quadrant Thrust Controller for Marine Propellers with Loss Estimation and Anti-Spin: Theory and Experiments*, Marine Technology, Vol. 46, N. 4, pp. 229-242, Oct. (2009).

[28] Rigby P., Pizarro O., Williams S., *Towards Geo-referencing AUV Navigation Through Fusion of USBL and DVL Measurements*, in Proceedings of MTS/IEEE OCEANS 2006, Boston, MA, USA (2006).

[29] Ristic B., Arulampalam S., Gordon N., editors, *Beyond the Kalman Filter*, Artech House Publishers, Boston, MA, USA (2004).

[30] Sayed A.H., editor, *Adaptive Filters*, Wiley and Sons, Hoboken, NJ, USA.

[31] University of Wisconsin, Green Bay website: *http://www.uwgb.edu*

[32] VectorNav Technologies: *http://www.vectornav.com*

[33] Wan E.A., Merwe R.V.D., *The Unscented Kalman Filter*, Wiley, pp. 221-280 (2001).

[34] Allotta B., Costanzi R., Fanelli F., Ridolfi A., *Single axis FOG aided attitude estimation algorithm for mobile robots*, Mechatronics, DOI: http:// dx.doi.org/10.1016/j.mechatronics.2015.06.012 (2015).

[35] Allotta B., Costanzi R., Ridolfi A., et al., *The ARROWS project: adapting and developing robotics technologies for underwater archaeology*, in Proceedings of IFAC Workshop on Navigation Guidance and Control of Underwater Vehicles (NGCUV 2015), Girona, Spain, (2015).